

1 **CERN - European Organization for Nuclear Research**

2  
3 **LCD-Note-2012-013**

4 **Prospects for the Measurement of the Top Mass in a**  
5 **Threshold Scan at CLIC**

6 Katja Seidel<sup>\*†</sup>, Frank Simon<sup>\*†</sup>, Michal Tesar<sup>\*</sup>

7 *\* Max-Planck-Institut für Physik, Munich, Germany,*

8 *† Excellence Cluster 'Universe', TU München, Garching, Germany*

9 August 30, 2012

10 **Abstract**

11 We present a study of the capability of CLIC to measure the top quark mass and the  
12 strong coupling constant in a scan of the top threshold. The analysis is based on full  
13 detector simulations of the CLIC\_ILD detector concept using Geant4, including re-  
14 alistic beam-induced background contributions from two photon processes. Event  
15 reconstruction is performed using a particle flow algorithm with stringent cuts to  
16 control the influence of background. With these simulations the signal and back-  
17 ground selection efficiencies are determined. Signal event yields as a function of  
18 energy are obtained using these efficiencies together with NNLO top pair cross-  
19 sections corrected for ISR and the CLIC beam energy spectrum. For comparison,  
20 the analysis is also performed with the ILC beam energy spectrum. We find that  
21 a statistical precision of 21 MeV of the top mass is achieved assuming fixed  $\alpha_s$ ,  
22 and a statistical uncertainty of 33 MeV for  $m_t$  and 0.0009 for  $\alpha_s$  is achieved in a  
23 combined extraction of both observables. At the ILC, the statistical uncertainties  
24 are between 10% and 20% smaller for the same integrated luminosity. In addition  
25 to the statistical uncertainties, systematic errors from theory and from the precision  
26 of  $\alpha_s$ , as well as the influence of the precision of the background description and of  
27 the understanding of the luminosity spectrum have been studied.

28	<b>Contents</b>	
29	<b>1 Introduction</b>	<b>3</b>
30	<b>2 Experimental Conditions at CLIC at the Top Threshold</b>	<b>3</b>
31	<b>3 Simulation Strategy</b>	<b>4</b>
32	3.1 Top Pair Production Cross Section . . . . .	4
33	3.1.1 Initial State Radiation . . . . .	4
34	3.1.2 Beam Energy Spectrum . . . . .	5
35	3.1.3 Combined Cross-Section . . . . .	5
36	3.2 Signal Selection Efficiency and Background Contamination . . . . .	6
37	3.3 Generation of Data Points . . . . .	8
38	<b>4 Results</b>	<b>9</b>
39	<b>5 Results for ILC beam conditions</b>	<b>10</b>
40	<b>6 Additional Systematic Studies</b>	<b>11</b>
41	<b>7 Conclusions</b>	<b>12</b>

## 1 Introduction

As the heaviest Standard Model particle, the top quark is of particular interest since it most strongly couples to the Higgs field and may provide sensitivity to Beyond the Standard Model physics. Experiments at  $e^+e^-$  colliders offer the possibility for a wide variety of studies involving top quarks, ranging from the precise measurement of top quark properties to the investigation of asymmetries providing large sensitivity to various New Physics models. Among those is the precise determination of the top quark mass, which is possible with two different techniques: through the direct reconstruction of top quarks from their decay products at energies above the production threshold, and through a scan of the top-pair production threshold. The latter technique has the advantage of providing the mass measurement in a theoretically well-defined scheme, while the former measurement can be performed essentially at arbitrary energies above threshold, however with potentially significant uncertainties due to non-perturbative contributions when transferring the measured invariant mass to a theoretically meaningful value. Progress has been made recently in establishing connections between the top mass parameters used in theory and the experimentally observable invariant mass of the decay products [1, 2], but theoretical uncertainties remain substantial.

In this note, we investigate the potential for the determination of the top quark mass from a measurement of the top-pair production cross-section at several energies around the threshold near 350 GeV, with a total integrated luminosity of up to  $100 \text{ fb}^{-1}$ . This study complements a previous CLIC study of top mass measurements at 500 GeV by means of a direct reconstruction of the invariant mass of the decay products, which showed that the invariant mass of the top quark can be determined with a precision of better than 100 MeV with  $100 \text{ fb}^{-1}$  in fully hadronic and semi-leptonic decays of the top pairs [3].

## 2 Experimental Conditions at CLIC at the Top Threshold

The Compact Linear Collider CLIC is a collider concept based on normal conducting accelerating cavities and two-beam acceleration, which is designed to provide up to 3 TeV collision energy. In a staged approach, a shorter, lower energy version would be operated initially, while construction is under way for the full energy phase.

In the present note, we study the case of a 500 GeV CLIC machine operated at energies close to the top pair production threshold. At 350 GeV, the rate of  $\gamma\gamma \rightarrow \text{hadrons}$  events is relatively small, with only 0.05 events per bunch crossing, down by almost an order of magnitude compared to 500 GeV collisions. The effect from pile-up of this background, in particular after the application of the particle flow object selection cuts, is thus very minor. In addition, the measurement at the top threshold is a measurement of the cross section, which requires the separation of signal and background events, but not the precise reconstruction of the invariant mass, which reduces the impact of the background on the analysis.

The detector model used in the present study is a variant of CLIC\_ILD [4], a detector concept based on Particle Flow event reconstruction. It consists of a low-mass, high-precision vertex detector and an inner silicon tracker, surrounded by a large-volume time projection chamber, followed by highly granular electromagnetic and hadronic calorimeters contained inside a 4 T

82 solenoidal magnet with instrumented flux return for muon identification. The detector design  
 83 is based on the ILD detector concept for the ILC, adapted to account for the higher energy  
 84 (3 TeV) and more severe background conditions at CLIC. This leads to an increased radius of the  
 85 innermost layer of the vertex detector, which sits at 31 mm compared to 16 mm in ILD at the ILC.  
 86 At 500 GeV, the background is significantly reduced compared to the 3 TeV case, permitting  
 87 modifications of the detector to optimize its performance for the lower collision energy. In  
 88 particular the innermost vertex detector layer for CLIC\_ILD can move in by 6 mm to a radius of  
 89 25 mm, improving flavor tagging at low momentum. To distinguish the modified detector design  
 90 from the 3 TeV design, the detector model is referred to as CLIC\_ILD\_CDR500.

## 91 **3 Simulation Strategy**

92 For the correct description of the cross-section near threshold, the inclusion of high-order QCD  
 93 contributions is necessary. Since no appropriate event generator publicly is available at present,  
 94 the study follows the strategy of earlier studies performed for the TESLA collider [5] by fac-  
 95 torising the simulation study into the determination of event selection efficiency and background  
 96 contamination and the calculation of the top-pair production threshold. In this approach, the sig-  
 97 nal selection and background rejection is determined using fully simulated top-pair signal events  
 98 as well as relevant background channels at a nominal center of mass energy of 352 GeV, slightly  
 99 above the production threshold for the selected top mass of 174 GeV. This energy is chosen to be  
 100 able to generate the events with PYTHIA, which requires a center-of-mass energy in excess of  
 101 twice the generator top mass. Data points along the threshold curve are then generated by taking  
 102 the signal cross section determined using NNLO calculations combined with the selection effi-  
 103 ciency, adding background events assuming a constant level over the considered energy range of  
 104 10 GeV as determined from the full simulations. In the following, more details are given on the  
 105 individual steps.

### 106 **3.1 Top Pair Production Cross Section**

107 The top-pair signal cross-section is determined using full NNLO calculations provided by the  
 108 code TOPPIK [6, 7]. The top mass input is set to 174 GeV in the 1S mass scheme [6]. The  
 109 strong coupling constant  $\alpha_s$  is taken to be 0.118. Since TOPPIK provides the cross section in  
 110 units of  $R$ , the ratio of  $\sigma(e^+e^- \rightarrow X)$  to  $\sigma(e^+e^- \rightarrow \mu^+\mu^-)$ , the appropriate conversion factor of  
 111 the energy-dependent cross section  $e^+e^- \rightarrow \mu^+\mu^-$  is applied in addition.

112 Since this cross section is calculated for the energy at the  $e^+e^-$  vertex, additional corrections  
 113 for initial state radiation (ISR) and for the beam energy spectrum of the accelerator have to be  
 114 applied, as discussed in the following.

#### 115 **3.1.1 Initial State Radiation**

116 ISR reduces the available collision energy  $E'$  due to the radiation of photons off the incoming  
 117 electron and positron prior to the collision. This effect in general lowers the signal cross-section,  
 118 since events are shifted to lower energies with typically a lower top-pair cross-section. The elec-  
 119 tron and positron “structure functions” are taken from the approximate YFS (Yennie-Frautschi-

120 Suura) solution as given in [8], which provides the normalized probability density for a given  
121 fraction of the lepton momentum  $x$  (ranging from 0 to 1) in the final collision.

122 For practical reasons, the folding of the ISR distribution with the theoretically calculated cross  
123 section is performed numerically. For this, a histogram of the structure function with 0.175 MeV  
124 wide bins is built, with the value in each bin taken by evaluating the approximate YFS solution at  
125 the bin center. The highest-energy bin is topped off to ensure correct normalization, accounting  
126 for the extreme increase in the structure function near 1. The folding is performed by evaluating  
127 100 000 randomly generated energy points with the individual beam energies distributed accord-  
128 ing to this histogram. The mean value of the cross-section of these 100 000 trials is taken as the  
129 ISR-corrected cross section at a given center-of-mass energy.

### 130 3.1.2 Beam Energy Spectrum

131 The beam energy distribution also influences the cross section as a function of collider energy.  
132 The beam energy distribution is roughly characterized by the width of the main luminosity peak  
133 and by a longer tail to lower energies from beamstrahlung. To be able to compare the impact of  
134 the different beam energy distributions of CLIC and ILC, spectra from both colliders, operated  
135 at 350 GeV, are used to calculate the final signal cross-section.

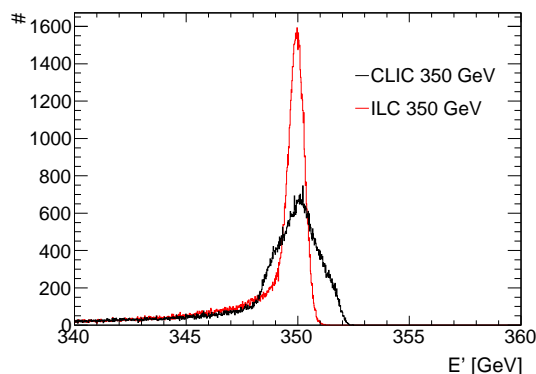


Figure 1: Beam energy spectrum for CLIC and ILC at 350 GeV.

136 Figure 1 shows the high-energy part of the beam energy spectrum of CLIC and ILC operated  
137 at 350 GeV. As for the case of ISR, the folding of the signal cross-section with the beam energy  
138 spectrum is performed numerically using 100 000 beam events at each energy point.

### 139 3.1.3 Combined Cross-Section

140 The final signal cross-section is obtained by combining the effects of ISR and of the beam  
141 energy spread. Using 100 000 trials per energy point with the collision energy determined from  
142 the beam energy distribution and ISR taken into account based on the resulting collision energy,  
143 the top pair cross section at both CLIC and ILC is determined based on the TOPPIK calculations.

144 Figure 2 shows the distribution of the real collision energy  $E'$  for CLIC and ILC for beam  
145 energy spectrum and ISR separately as well as the resulting combined spectrum. The effect on

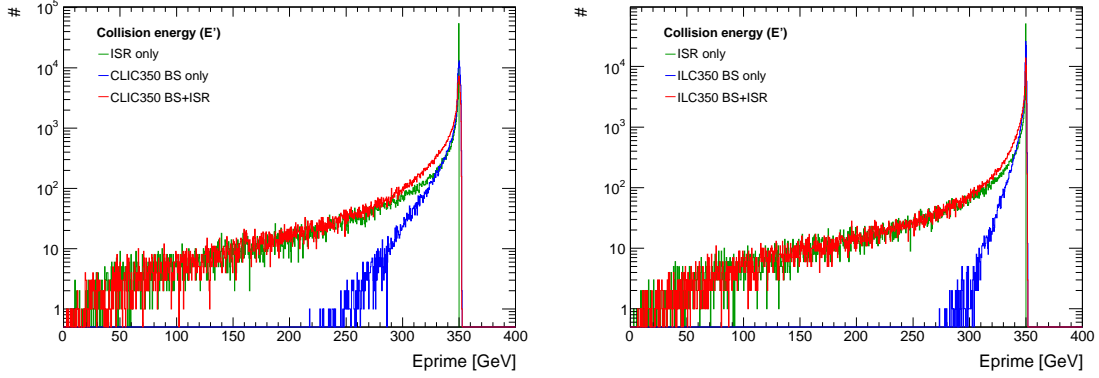


Figure 2:  $E'$  distribution taking ISR and beam energy spectrum (CLIC (left) and ILC (right)) into account.

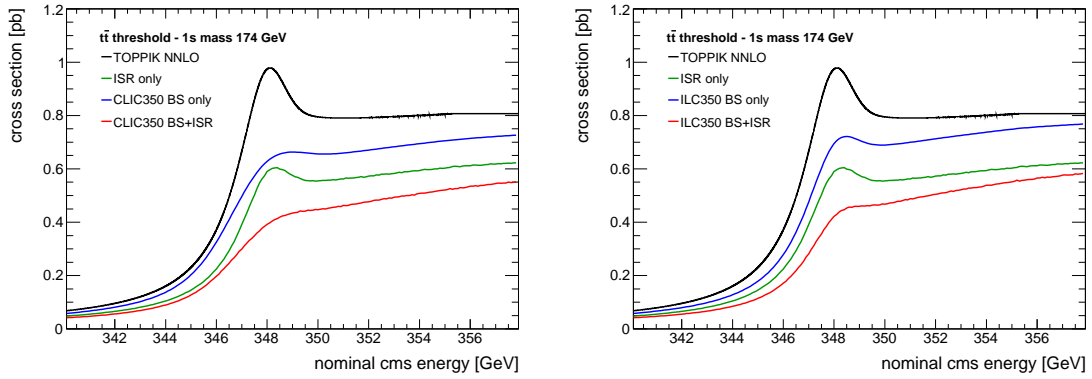


Figure 3: Top pair production cross-section from theory calculations, with beam energy spectrum and ISR as well as for all effects combined for both CLIC (left) and ILC (right).

146 the top pair production cross-section is shown in Figure 3. The cross-section with all effects  
 147 included is used to determine the signal yield as a function of nominal collision energy in the  
 148 subsequent analysis steps.

### 149 3.2 Signal Selection Efficiency and Background Contamination

150 The event selection efficiency and the background contributions, mainly from di- and tri-boson  
 151 production, are determined using events generated with PYTHIA at a collision energy of 352 GeV  
 152 with a top mass of 174 GeV. These events are fully simulated including pile-up from  $\gamma\gamma \rightarrow$   
 153 hadrons background. For signal identification and background rejection the same technique  
 154 as for the 500 GeV top mass study [3] is used. The top pair events are identified in the  
 155 fully hadronic decay mode  $t\bar{t} \rightarrow W^+bW^-\bar{b} \rightarrow q\bar{q}q\bar{q}b\bar{b}$  and in the semi-leptonic mode  $t\bar{t} \rightarrow$   
 156  $W^+bW^-\bar{b} \rightarrow q\bar{q}l^\pm\nu_l b\bar{b}$ , ( $l = e, \mu$ ). The events are clustered into six or four jets depending

157 on the number of identified isolated leptons. A kinematic fit with constraints on overall energy,  
 158 on the difference of the two top masses and on the mass of the intermediate  $W$  bosons is used to  
 159 form the top candidates. The fit also provides powerful background rejection, since most back-  
 160 ground events fail the kinematic fit. Additional background reduction is obtained with a binned  
 161 likelihood using flavor tagging and other event variables to discriminate signal from background.

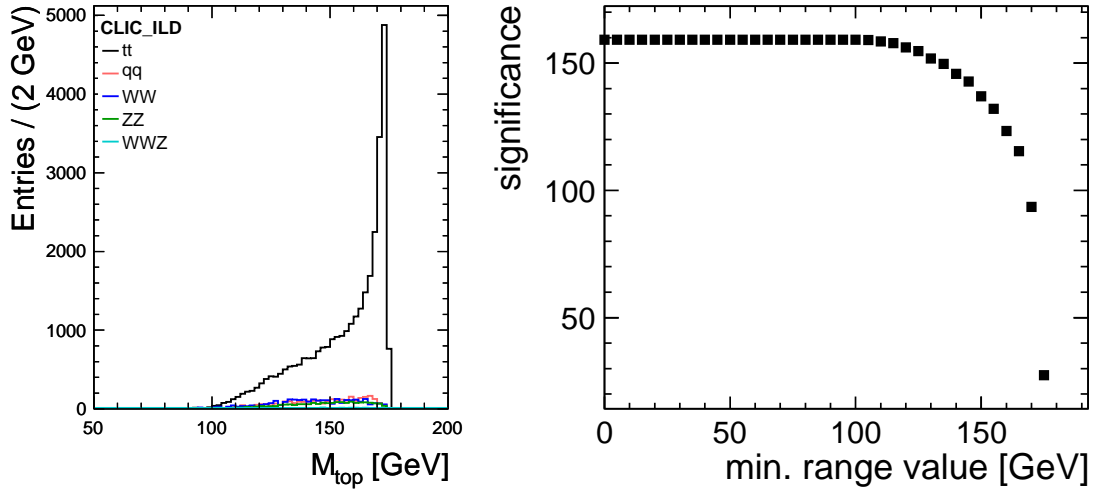


Figure 4: Reconstructed top quark mass for accepted events. Signal as well as each of the back-  
 grounds are shown separately (left). Signal significance as a function of the value of a  
 potential invariant mass cut above threshold for a top pair production cross-section of  
 $450 \text{ fb}^{-1}$  (right).

162 No further selection based on the reconstructed top quark mass is performed since this does  
 163 not provide a substantial additional background rejection, while it would add potential system-  
 164 atic uncertainties from the additional cut. Figure 4 shows the reconstructed invariant mass dis-  
 165 tribution for top quark candidates after all selections for accepted signal and background events,  
 166 as well as the signal significance above threshold (assuming a signal cross-section of  $450 \text{ fb}$ )  
 167 as a function of a possible invariant mass cut. Overall, a signal selection efficiency of 70.2% is  
 168 achieved, with an efficiency in excess of 90% for the selected fully-hadronic and semi-leptonic  
 169 decay modes. For the major background channels, the cross-section is reduced by two to three  
 170 orders of magnitude. Table 1 summarizes the signal and background cross-sections before and  
 171 after selection.

172 Even though the study is performed using the CLIC\_ILD detector model and CLIC back-  
 173 ground conditions, the conclusions drawn about the signal selection efficiency and background  
 174 contamination also apply to ILC and the ILD detector. In terms of detector model, the most  
 175 relevant difference is the radius of the innermost vertex detector layer, which is larger at CLIC  
 176 due to the higher background level of incoherent  $e^+e^-$  pairs. For the identification of  $t\bar{t}$  events,  
 177  $b$ -tagging is crucial, but not the separation of charm and bottom. Thus, the differences in per-  
 178 formance of the two detector models are expected to be negligible for this analysis. The same

Table 1: Signal and considered physics background processes, with their cross section calculated for CLIC at 352 GeV before and after event selection. The combined background cross-section after selection is 78 fb.

type	$e^+e^- \rightarrow$	$\sigma$ at 352 GeV	selected $\sigma$
Signal ( $m_{\text{top}} = 174 \text{ GeV}$ )	$t\bar{t}$	450 fb	316 fb
Background	$q\bar{q}$	25.2 pb	28 fb
Background	$WW$	11.5 pb	28 fb
Background	$ZZ$	865 fb	19 fb
Background	$WWZ$	10 fb	3 fb

179 also applies for the background rejection. Thus, the selection efficiencies and background levels  
 180 determined for CLIC are also used for a study of a threshold scan at ILC.

### 181 3.3 Generation of Data Points

182 Simulated data points are generated by taking the ISR and beam spectrum corrected top pair  
 183 cross-section at the desired energy to calculate the nominal number of events expected. The  
 184 simulated number of signal events is determined on a random basis following a gaussian distri-  
 185 bution with the mean set to the nominal number of events and the standard deviation given by  
 186 the square root of that number. With the same method, background events are added, using a  
 187 constant cross-section of 78 fb as discussed above. It is assumed that the nominal background  
 188 contribution is well known both from theory and from measurements below threshold, so the  
 189 nominal number of background events is subtracted from the signal, leaving just the statistical  
 190 variations on top of the signal data with its own statistical uncertainty.

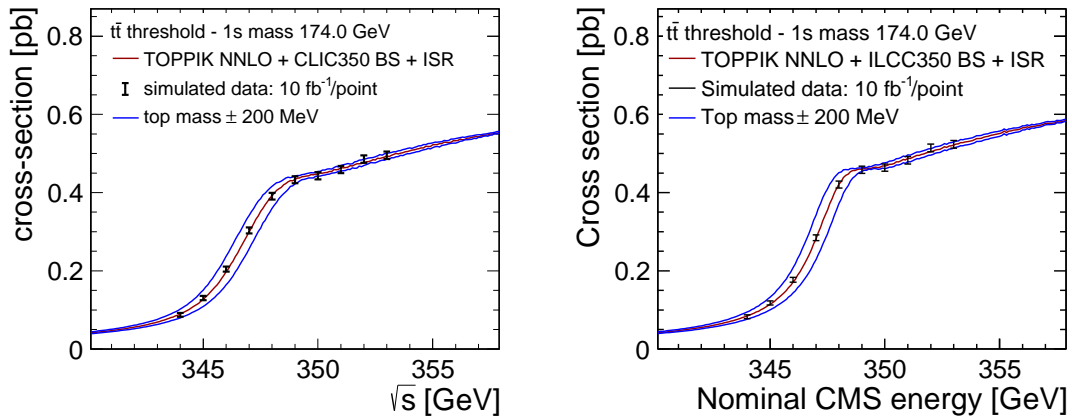


Figure 5: Background-subtracted simulated cross-section measurements for  $10 \text{ fb}^{-1}$  per data point, together with the cross-section for the generator mass of 174 GeV as well as for a shift in mass of  $\pm 200 \text{ MeV}$  for both CLIC (left) and ILC (right).



191 In the present analysis, we assume a threshold scan with 10 data points with an integrated  
 192 luminosity of  $10 \text{ fb}^{-1}$  each. The measurement points are spaced by 1 GeV. Figure 5 shows  
 193 simulated data points for CLIC and for ILC.

## 194 4 Results

195 Two extractions of the top mass are being considered here: A one-dimensional template fit  
 196 performed by comparing the simulated data with theory curves calculated in 50 MeV steps in  
 197 top mass assuming  $\alpha_s$  is known, and a two-dimensional template fit in top mass and  $\alpha_s$  for a  
 198 simultaneous determination of the top mass and the strong coupling constant. The measured  
 199 top mass, and  $\alpha_s$  in the case of the 2D fit, is given by the minimum of a parabolic fit to the  
 200  $\chi^2$  distribution of the different templates. The statistical uncertainty is taken from the standard  
 201 deviation of the measured mass in 5000 trials with different simulated data points.

202 In the 1D fit, two main sources of systematic uncertainties are considered: A theory un-  
 203 certainty taken as an overall normalization uncertainty of the calculated cross section, and an  
 204 uncertainty from the knowledge of  $\alpha_s$ , which is assumed to be known in the 1D fit. For the  
 205 theory uncertainty, two levels are considered: A normalization uncertainty of 3%, assumed as  
 206 a reasonably conservative estimate of current theory uncertainties [9], and an uncertainty of 1%  
 207 optimistically assumed to be achievable with additional theoretical work in time for experiments  
 208 at linear colliders. To determine the systematic error due to  $\alpha_s$ , the current uncertainty of the  
 209 world average of 0.0007 is assumed. The interpretation of the data points above threshold is  
 210 particularly sensitive to the overall theory normalization uncertainty and to the strong coupling  
 211 constant. In the 1D fit, uncertainties can thus be somewhat reduced by just considering the first  
 212 six data points from 344 GeV to 349 GeV, without a reduction of the statistical sensitivity to the  
 213 top mass. Table 2 summarizes the results.

Table 2: Results summary for the 1D top mass determination with a threshold scan at CLIC. For  
 the systematic uncertainty originating from  $\alpha_s$ , the current error on the world average  
 of 0.0007 is assumed.

1S top mass 1D fit			
measurement	stat. error	theory syst. (1%/3%)	$\alpha_s$ syst.
six point scan	21 MeV	15 MeV / 45 MeV	20 MeV
ten point scan	21 MeV	18 MeV / 54 MeV	21 MeV

214 Since the shape of the cross-section as a function of energy depends both on the top mass  
 215 and on the strong coupling constant, a simultaneous determination of both is possible with a  
 216 two-dimensional template fit. Figure 6 shows the resulting precision, and shows the clear cor-  
 217 relation of the two variables. Since sensitivity to  $\alpha_s$  also comes in through the higher-energy  
 218 scan points, a reduced scan with six points along the strongly rising region of the cross-section  
 219 lead to significantly increased uncertainties. In the case of the 2D fit, only the theory uncertainty  
 220 is considered as a source for systematic uncertainties in the fit. The results are summarized in  
 221 Table 3.

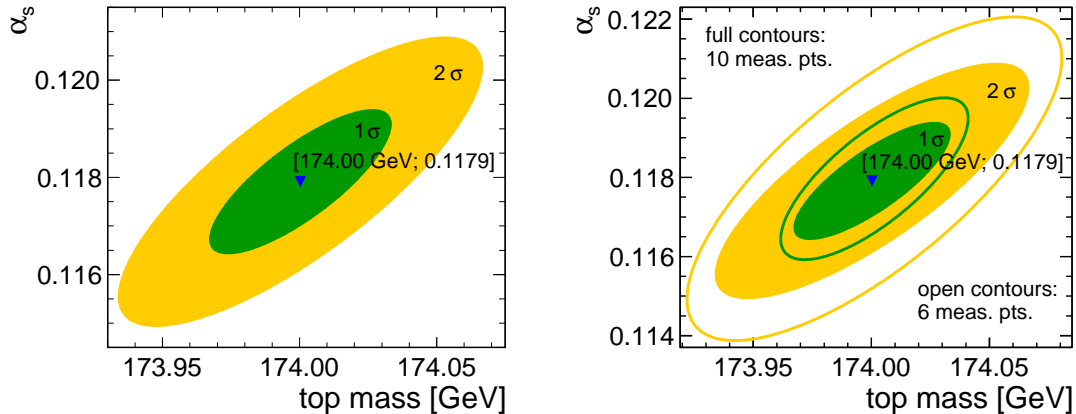


Figure 6: Simultaneous fit of the top mass and the strong coupling constant, showing the correlation of the two variables and the achieved precision (left). Difference in precision of top mass and  $\alpha_s$  fit using just the first 6 points in the threshold scan or all 10 points (right).

Table 3: Results summary for the 2D simultaneous top mass and  $\alpha_s$  determination with a threshold scan at CLIC.

1S top mass and $\alpha_s$ combined 2D fit				
measurement	$m_t$ stat. error	$m_t$ th. syst. (1%/3%)	$\alpha_s$ stat. error	$\alpha_s$ th. syst. (1%/3%)
six point scan	39 MeV	2 MeV / 4 MeV	0.0014	0.0008 / 0.0020
ten point scan	33 MeV	6 MeV / 13 MeV	0.0009	0.0009 / 0.0022

## 222 5 Results for ILC beam conditions

223 The influence of the beam energy spectrum of the accelerator is studied by repeating the analysis using the ILC beam energy spectrum, as discussed in Section 3.1.2. The faster rise of the cross section due to the sharper main luminosity peak is expected to lead to somewhat reduced statistical uncertainties on the top mass for a given integrated luminosity due to increased differences between different mass hypotheses in the threshold region. As for the CLIC analysis, an integrated luminosity of  $10 \text{ fb}^{-1}$  per point is assumed. The same one- and two-dimensional fits of  $m_t$  and  $m_t$  and  $\alpha_s$  combined are also performed for data points generated with the ILC beam spectrum. For simplicity, only the ten point fits are performed, and the systematic errors taking into account the theory normalization uncertainty and the uncertainty of  $\alpha_s$  are not determined. It is however expected that these uncertainties are quantitatively very similar to the CLIC case.

232 Table 4 summarizes the results of both 1D and 2D fits, while Figure 7 shows the results of the combined extraction of the top mass and the strong coupling constant, illustrating the statistical uncertainty and the correlation of the two variables. In comparison to the statistical precision achieved assuming the CLIC beam energy spectrum, in the ILC case a 15% smaller uncertainty is observed in the 1D top mass fit, and a 20% smaller uncertainty on the top mass and a 10%

Table 4: Results summary for the 1D top mass fit and the 2D simultaneous top mass and  $\alpha_s$  determination with a threshold at ILC.

ILC 1D 1S top mass and 2D 1S top mass and $\alpha_s$ combined fit		
measurement	$m_t$ stat. error	$\alpha_s$ stat. error
ten point scan 1D fit	18 MeV	-
ten point scan 2D fit	27 MeV	0.0008

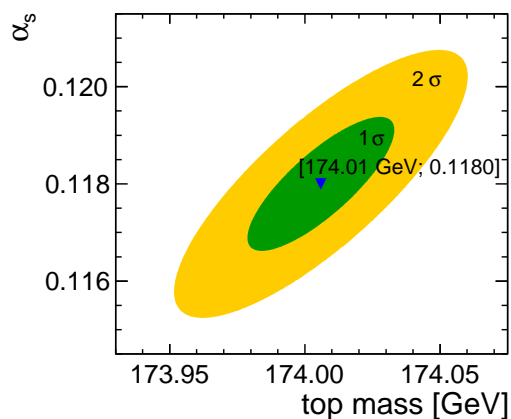


Figure 7: Simultaneous fit of the top mass and the strong coupling constant for data points simulated with the ILC beam energy spectrum, showing the correlation of the two variables and the achieved precision.

238 smaller uncertainty on  $\alpha_s$  is obtained in the combined extraction. Compared to the systematic  
 239 uncertainties originating from theory and from the precision of the strong coupling constant  
 240 these differences are negligible.

## 241 6 Additional Systematic Studies

242 In addition to the theory uncertainties and the uncertainty of  $\alpha_s$  in the case of the 1D fit, addi-  
 243 tional potential sources for systematic errors were studied.

244 A potential dependence of the result on the precise choice of energy values for the scan in  
 245 relation to the top mass was excluded by shifting the measurement points to higher energies by  
 246 0.5 GeV without a significant change in the determined mass and  $\alpha_s$  values.

247 The precise knowledge of the non-top background after event selection is crucial for the mea-  
 248 surement of the signal cross section. The effect of an imperfect background description is studied  
 249 by subtracting 5% and 10% too little or too much background before the fit. The 5% variation  
 250 results in a 20 MeV shift in the top mass and 0.0005 in  $\alpha_s$ , in both cases approximately two  
 251 thirds of the statistical uncertainty. Subtracting only 90% of the background leads to a shift of  
 252 twice the size, but also significantly reduces the stability of the template fit. Subtracting 110% of

253 the background leads to a 30 MeV shift of the top mass and a shift of 0.0014 in  $\alpha_s$ . This shows  
254 that an understanding of the background contamination on the level of 5% or better is important  
255 to keep systematic effects substantially below the statistical uncertainties.

256 The knowledge of the beam energy spectrum is very important for the correct description of  
257 the signal cross section, and thus also for the precision of the template fit. A full study has not  
258 yet been performed, but a very preliminary first study indicates that already a 20% uncertainty of  
259 the RMS width of the main luminosity peak results in top mass uncertainties of approximately  
260 75 MeV, far in excess of the statistical uncertainties. Further studies to quantify the effects of  
261 realistic uncertainties of the beam energy spectrum are needed.

## 262 7 Conclusions

263 In this study, we have investigated the achievable precision of the top quark mass with a thresh-  
264 old scan at CLIC. Compared to the direct measurement of the invariant mass of the top quark  
265 decay products the threshold scan has the advantage that the mass is directly determined in  
266 a theoretically well-defined mass definition. The study uses event selection efficiencies and  
267 background contaminations from fully simulated events including the effects of the CLIC beam  
268 spectrum and  $\gamma\gamma \rightarrow$  hadrons backgrounds and top pair signal cross-sections from NNLO cal-  
269 culations corrected for ISR and the beam energy spectrum. With an integrated luminosity of  
270  $100 \text{ fb}^{-1}$  divided across ten data points spaced by 1 GeV, a statistical precision of the top quark  
271 mass in the 1S scheme of 33 MeV is obtained in a combined fit together with the strong coupling  
272 constant, which is determined with a precision of 0.0009. A one-dimensional fit with fixed  $\alpha_s$   
273 yields a precision of 21 MeV. Using the ILC beam energy spectrum instead results in 15% to  
274 20% smaller uncertainties on the mass and in a 10% smaller uncertainty of the strong coupling  
275 constant. Combined systematic uncertainties from theory and background control are expected  
276 to be of similar order as the statistical errors. Together with a previous study of top quark mass  
277 measurements from direct reconstruction of the decay products this study demonstrates that pre-  
278 cision top measurements are possible at CLIC both at and above threshold.

## References

- 279
- 280 [1] S. Fleming, A. H. Hoang, S. Mantry, and I. W. Stewart. Jets from massive unstable particles:  
281 Top-mass determination. *Phys.Rev.*, vol. D77 p. 074010, 2008.
- 282 [2] S. Fleming, A. H. Hoang, S. Mantry, and I. W. Stewart. Top Jets in the Peak Region:  
283 Factorization Analysis with NLL Resummation. *Phys.Rev.*, vol. D77 p. 114003, 2008.
- 284 [3] K. Seidel, S. Poss, and F. Simon. Top quark pair production at a 500 GeV CLIC collider,  
285 2011. CERN LCD-2011-026.
- 286 [4] A. Münnich and A. Sailer. The CLIC ILD CDR Geometry for the CDR Monte Carlo Mass  
287 Production. *LCD-Note-2011-002*, 2011.
- 288 [5] M. Martinez and R. Miquel. Multiparameter fits to the  $t\bar{t}$  threshold observables at a future  
289  $e^+e^-$  linear collider. *Eur. J. Phys.*, vol. C27 pp. 49–55, 2003. hep-ph/0207315.
- 290 [6] A. H. Hoang and T. Teubner. Top quark pair production close to threshold: Top mass, width  
291 and momentum distribution. *Phys. Rev.*, vol. D60 p. 114027, 1999. CERN-TH-99-59,  
292 DESY-99-047, hep-ph/9904468.
- 293 [7] A. H. Hoang and T. Teubner. Top quark pair production at threshold: Complete next-to-  
294 next-to-leading order relativistic corrections. *Phys. Rev.*, vol. D58 p. 114023, 1998. UCSD-  
295 PTH-98-01, DESY-98-008, hep-ph/9801397.
- 296 [8] M. Skrzypek and S. Jadach. Exact and approximate solutions for the electron nonsinglet  
297 structure function in QED. *Z.Phys.*, vol. C49 pp. 577–584, 1991.
- 298 [9] A. Hoang and M. Stahlhofen. NNLL Top-Antitop Production at Threshold. 2011.  
299 arXiv:1111.4486 [hep-ph].